

Global simulation of plasma series resonance effect in radio frequency capacitively coupled Ar/O_2 plasma

Xue Bai(白雪), Hai-Wen Xu(徐海文), Chong-Biao Tian(田崇彪), Wan Dong(董婉), Yuan-Hong Song(宋远红), and You-Nian Wang(王友年)

Citation: Chin. Phys. B, 2023, 32 (**12**): 125203. DOI: 10.1088/1674-1056/ace427
Journal homepage: http://cpb.iphy.ac.cn; http://iopscience.iop.org/cpb

What follows is a list of articles you may be interested in

Efficient ion acceleration driven by a Laguerre-Gaussian laser in near-critical-density plasma

Jia-Xiang Gao(高嘉祥), Meng Liu(刘梦), and Wei-Min Wang(王伟民)
Chin. Phys. B, 2023, 32 (**10**): 105202. DOI: 10.1088/1674-1056/ace428

Effect of sharp vacuum-plasma boundary on the electron injection and acceleration in a few-cycle laser driven wakefield

Guo-Bo Zhang(张国博), Song Liu(刘松), De-Bin Zou(邹德滨), Ye Cui(崔野), Jian-Peng Liu(刘建鹏), Xiao-Hu Yang(杨晓虎), Yan-Yun Ma(马燕云), and Fu-Qiu Shao(邵福球)
Chin. Phys. B, 2023, 32 (**9**): 095202. DOI: 10.1088/1674-1056/acdc0c

Theoretical analyses on the one-dimensional charged particle transport in a decaying plasma under an electrostatic field

Yao-Ting Wang(汪耀庭), Xin-Li Sun(孙鑫礼), Lan-Yue Luo(罗岚月), Zi-Ming Zhang(张子明), He-Ping Li(李和平), Dong-Jun Jiang(姜东君), and Ming-Sheng Zhou(周明胜)
Chin. Phys. B, 2023, 32 (**9**): 095201. DOI: 10.1088/1674-1056/ace033

Intense low-noise terahertz generation by relativistic laser irradiating near-critical-density plasma

Shijie Zhang(张世杰), Weimin Zhou(周维民), Yan Yin(银燕), Debin Zou(邹德滨), Na Zhao(赵娜), Duan Xie(谢端), and Hongbin Zhuo(卓红斌)
Chin. Phys. B, 2023, 32 (**3**): 035201. DOI: 10.1088/1674-1056/ac872c

Effect of kinetic ions on the toroidal double-tearing modes

Ruibo Zhang(张睿博), Lei Ye(叶磊), Yang Chen, Nong Xiang(项农), and Xiaoqing Yang(杨小庆)
Chin. Phys. B, 2023, 32 (**2**): 025203. DOI: 10.1088/1674-1056/ac7f89

Speeding-up direct implicit particle-in-cell simulations in bounded plasma by obtaining future electric field through explicitly propulsion of particles

Haiyun Tan(谭海云)[1,2], Tianyuan Huang(黄天源)[1,2], Peiyu Ji(季佩宇)[2,3], Mingjie Zhou(周铭杰)[1,2], Lanjian Zhuge(诸葛兰剑)[4], and Xuemei Wu(吴雪梅)[1,2,†]

[1] *School of Physical Science and Technology & Collaborative Innovation Center of Suzhou Nano Science and Technology, Soochow University, Suzhou* 215006, *China*

[2] *Key Laboratory of Advanced Optical Manufacturing Technologies of Jiangsu Province & Key Laboratory of Modern Optical Technologies of Education Ministry of China, Soochow University, Suzhou* 215006, *China*

[3] *School of Optoelectronic Science and Engineering, Soochow University, Suzhou* 215006, *China*

[4] *Analysis and Testing Center, Soochow University, Suzhou* 215123, *China*

(Received 7 June 2023; revised manuscript received 25 July 2023; accepted manuscript online 28 August 2023)

The direct implicit particle-in-cell is a powerful kinetic method for researching plasma characteristics. However, it is time-consuming to obtain the future electromagnetic field in such a method since the field equations contain time-dependent matrix coefficients. In this work, we propose to explicitly push particles and obtain the future electromagnetic field based on the information about the particles in the future. The new method retains the form of implicit particle pusher, but the future field is obtained by solving the traditional explicit equation. Several numerical experiments, including the motion of charged particle in electromagnetic field, plasma sheath, and free diffusion of plasma into vacuum, are implemented to evaluate the performance of the method. The results demonstrate that the proposed method can suppress finite-grid-instability resulting from the coarse spatial resolution in electron Debye length through the strong damping of high-frequency plasma oscillation, while accurately describe low-frequency plasma phenomena, with the price of losing the numerical stability at large time-step. We believe that this work is helpful for people to research the bounded plasma by using particle-in-cell simulations.

Keywords: particle-in-cell, direct implicit simulation, finite-grid-instability

PACS: 52.80.Pi, 52.27.Aj, 52.65.Rr **DOI:** 10.1088/1674-1056/acf449

1. Introduction

Low-temperature bounded plasmas, such as capacitively coupled plasmas (CCPs) or magnetron plasmas, have generated significant research interest due to their applications in film preparation, hi-tech industries, materials surface treatment, and other areas.[1–3] Charged particles in plasmas play significant roles in plasma-based material processing. Therefore, researching the particle dynamics and microscopic physical processes in plasma is crucial for optimizing the plasma technological processes.

Particle-in-cell (PIC) methods are useful simulation tools for the kinetics study of plasma. At present, explicit PIC algorithms is perhaps the most widely used method.[4–8] Such the method calculates the electromagnetic (EM) field based on the known information of the particles, at the currently calculation step. Explicit PIC algorithms require very small spatial step Δx and time-step Δt to obtain the desired numerical stability. In practice, one needs $\Delta x < \lambda_{\mathrm{De}}$ and $\omega_{\mathrm{pe}}\Delta t < 0.2$,[9] where the λ_{De} and ω_{pe} represent the electron Debye length and the electron plasma frequency, respectively. In addition, hundreds of macro-particles per cell are needed to reduce the statistical error originating from the sampling of the distribution function by macro-particles.[10] As a result, a very large number of meshes, calculation-steps and macro-particles are needed in traditional explicit PIC methods, and it is time-consuming to use explicit PIC methods for the kinetics study of plasma.

Despite the aforementioned challenges, explicit PIC methods remain attractive, especially since there is a desire to address high-frequency plasma oscillations in many situations. Several methods have been proposed to improve the calculation speed of the explicit PIC. Firstly, parallel computation using multiple processors or GPUs can be used to accelerate the task.[11–13] Speed gains can also be achieved through mathematical and physical methods. For example, a large time-step $\Delta t_{\mathrm{i}} \gg \Delta t_{\mathrm{e}}$ for heavy ions can be used since ions are much heavier than electrons and their macroscopic properties can be analyzed on a longer timescale.[14] Here, the subscripts 'i' and 'e' represent ion and electron, respectively. Another method is the scaling principle, which involves the scaling of mass of ions, vacuum permittivity and geometric size of the system.[15–17] Such the method is widely used in the research of Hall thrusters. Besides, different spatial steps can be used in different plasma regions. For instance, small spatial step and time-step should be employed near the plasma sheath to track fast electrons and resolve the sheath, whereas larger steps can be used in the bulk region.[18]

†Corresponding author. E-mail: xmwu@suda.edu.cn

© 2023 Chinese Physical Society and IOP Publishing Ltd

On the other hand, if the high-frequency electron plasma oscillation is not the main physical process that determines plasma character, then implicit methods can be used to accelerate the computing by using large spatial and temporal steps with coarse resolution in Debye length and electron oscillation. The traditional implicit methods, such as direct implicit methods[19] or implicit-moment methods,[20] are developed to relax the numerical stability constraint of explicit PIC on time-step. Further research has shown that a large spatial step is also allowed in these implicit PICs because the high-frequency electron oscillation causing finite-grid-instability is damped.[21] In recent years, some implicit methods with energy conservation have been developed,[22–24] which can relax the requirements of numerical stability on time-step and spatial step significantly.

Implicit methods are attractive as they allow PIC simulations to be run with large time-step and spatial step. However, their performance is limited in researching bounded plasma due to several reasons. Firstly, it is time-consuming to solve the implicit field equations for the traditional implicit PIC since the equations contain time-dependent coefficients.[25] On the other hand, the particle pusher in the implicit PICs with energy conservation is sophisticated to maintain total energy conservation.[26] Moreover, the spatial step must be smaller than one-fifth of sheath thickness to resolve plasma sheath,[21] which means that very large spatial step is not allowed, and a small time-step is also required to meet the Courant–Friedrichs–Lewy (CFL) condition.[9] In general, the implicit PIC methods relax the constraints on time-step and spatial step by a factor of ~ 10.[26]

Therefore, the ideal PIC method for researching bounded plasma should simulate plasma behavior accurately, using the spatial step large enough to resolve plasma sheath and the time-step large enough to track fast electron group. In addition, it should have efficient field solvers and particle pushers, and be compatible with existing PIC frameworks to utilize various speed-up techniques. This work proposes a PIC method with damping of high-frequency electron oscillation, which obtains the future fields by solving traditional explicit field equations with constant matrix coefficient and uses the same particle pusher as that used in the direct implicit PIC method. Section 2 briefly reviews the theoretical background of the explicit and direct implicit PIC methods, while Section 3 describes the algorithm of the proposed damped PIC. In Section 4, several numerical experiments are implemented to evaluate the performance of the new method. The last part is a summary and a description of the future work.

2. Theoretical background

In this section, we will review two traditional PIC methods, namely explicit PIC (EXPIC) and direct implicit PIC (DIMPIC). We begin with a charged particle having velocity $\boldsymbol{v}^{n-1/2}$, locating at position $\boldsymbol{x}^n$, at time step n. The central difference equations of motion for the charged particle are then used to compute the position and velocity at next time step, as follows:[3]

$$\begin{aligned}\frac{\boldsymbol{v}^{n+1/2}-\boldsymbol{v}^{n-1/2}}{\Delta t} &= \boldsymbol{a}^n(\boldsymbol{x}^n)+\frac{1}{2}(\boldsymbol{v}^{n+1/2}+\boldsymbol{v}^{n-1/2})\times\boldsymbol{\Omega}^n,\\ \frac{\boldsymbol{x}^{n+1}-\boldsymbol{x}^n}{\Delta t} &= \boldsymbol{v}^{n+1/2},\end{aligned} \tag{1}$$

here Δt is the time-step, $\boldsymbol{a}^n(\boldsymbol{x}^n)$ and $\boldsymbol{\Omega}^n=(q/m)\boldsymbol{B}^n(\boldsymbol{x}^n)$ represent the electric field acceleration and the cyclotron frequency of the particle at $\boldsymbol{x}^n$, respectively, where $\boldsymbol{B}^n$ represents the magnetic field and q/m represents charge mass ratio of the particle. For convenience, we only consider electrostatic case.

2.1. Explicit PIC

It is both convenient and intuitive to track the motion of the particle by using EXPIC. In this method, the position $\boldsymbol{x}^n$ is first used to obtain the charge density ρ^n at a given mesh using some interpolation methods. Next, the electric field $\boldsymbol{E}^n$ at the current time step is obtained by solving the explicit Poisson equation with source term of ρ^n, which in turn is used to update the velocity and position. Finally, the solution is completed, and the calculation proceeds to the next time step. The algorithm of EXPIC is as follows:

(i) $\boldsymbol{x}^n \to \rho^n$ (interpolation of charge density from the particles);

(ii) solving the explicit Poisson equation to obtain $\boldsymbol{E}^n$ at the mesh, that is,

$$\nabla^2\phi^n = -\rho^n/\varepsilon_0, \tag{2}$$

where ϕ represents potential and ε_0 is the permittivity of vacuum;

(iii) $\boldsymbol{a}^n(\boldsymbol{x}^n)=(q/m)\boldsymbol{E}^n(\boldsymbol{x}^n)$ (interpolation of the field from mesh);

(iv) $\boldsymbol{v}^{n+1/2}=\boldsymbol{v}^{n-1/2}+\boldsymbol{a}^n(\boldsymbol{x}^n)\Delta t+(\Delta t/2)[(\boldsymbol{v}^{n+1/2}+\boldsymbol{v}^{n-1/2})\times\boldsymbol{\Omega}^n]$;

(v) $\boldsymbol{x}^{n+1}=\boldsymbol{x}^n+\boldsymbol{v}^{n+1/2}\Delta t$;

(vi) $\boldsymbol{\Omega}^{n+1}=(q/m)\boldsymbol{B}^{n+1}(\boldsymbol{x}^{n+1})$ (interpolation of the field from mesh).

The dispersion relationship for the electrostatic Langmuir wave with frequency of $\omega_{\rm pe}$ predicted by the EXPIC is expressed as follows:[27]

$$\sin(\omega\Delta t/2)=\pm\omega_{\rm pe}\Delta t/2, \tag{3}$$

where ω represents the frequency predicted by numerical calculation. As shown in Eq. (3), the EXPIC is numerically unstable when $\omega_{\rm pe}\Delta t>2$. In addition, the EXPIC is a method that cannot damp wave oscillation. Thus, using a large spatial step here with coarse resolution in Debye length will result in finite-grid-instability since the numerical oscillations enhance gradually.[3]

2.2. Direct implicit PIC

The DIMPIC is developed to relax the numerical stability constraint on time-step. In such method, equation (1) is modified as follows:[28]

$$\begin{aligned}&\frac{\boldsymbol{v}^{n+1/2}-\boldsymbol{v}^{n-1/2}}{\Delta t}\\&=\frac{1}{2}\left[\boldsymbol{a}^{n+1}\left(\boldsymbol{x}^{n+1}\right)+\overline{\boldsymbol{a}^{n-1}}+\left(\boldsymbol{v}^{n+1/2}+\boldsymbol{v}^{n-1/2}\right)\times\boldsymbol{\Omega}^{n}\right],\\&\frac{\boldsymbol{x}^{n+1}-\boldsymbol{x}^{n}}{\Delta t}=\boldsymbol{v}^{n+1/2},\end{aligned}\tag{4}$$

here $\overline{\boldsymbol{a}^{n-1}}=(\boldsymbol{v}^{n-1/2}-\boldsymbol{v}^{n-3/2})/\Delta t$ represents the time-averaged electric filed acceleration of the particle at previous time step. It can be seen from Eq. (4) that the actual value of $\boldsymbol{a}^{n}$ is substituted with a weighted value of $\boldsymbol{a}^{n+1}$ and $\overline{\boldsymbol{a}^{n-1}}$, that is,

$$\boldsymbol{a}^{n}(\boldsymbol{x}^{n})=\frac{1}{2}\boldsymbol{a}^{n+1}(\boldsymbol{x}^{n+1})+\frac{1}{2}\overline{\boldsymbol{a}^{n-1}},\tag{5}$$

where $\overline{\boldsymbol{a}^{n-1}}$ is a known quantity. However, $\boldsymbol{a}^{n+1}(\boldsymbol{x}^{n+1})$ related to the position $\boldsymbol{x}^{n+1}$ at next time step is an unknown quantity because one still does not know $\boldsymbol{x}^{n+1}$ until now.

If one wishes to calculate $\boldsymbol{a}^{n}(\boldsymbol{x}^{n})$ accurately by using $\boldsymbol{a}^{n+1}(\boldsymbol{x}^{n+1})$, it is necessary to use $\boldsymbol{x}^{n+1}$ to obtain ρ^{n+1}, which in turn can be used to calculate $\boldsymbol{E}^{n+1}$. However, this process is often nearly impossible, and one must rely on some approximate methods. To obtain $\boldsymbol{a}^{n+1}(\boldsymbol{x}^{n+1})$, DIMPIC uses a method proposed by Langdon *et al.*,[29] in which the approximate field $\boldsymbol{E}^{n+1}$ is first obtained by solving the implicit Poisson equation. Then, the approximate $\boldsymbol{a}^{n+1}(\boldsymbol{x}^{n+1})$ is obtained by some interpolation algorithms.

In DIMPIC, the push process is split into two to separate the effects of the future electric field from those of known fields. The first push process uses $\overline{\boldsymbol{a}^{n-1}}$ to pre-push the particle and obtain the source terms for solving the implicit Poisson equation, which in turn gives $\boldsymbol{a}^{n+1}(\boldsymbol{x}^{n+1})$. Then the second push process uses $\boldsymbol{a}^{n+1}(\boldsymbol{x}^{n+1})$ to final-push the particle and complete the solution at the current time step. The algorithm for DIMPIC can be summarized as follows:

Pre-pusher:

(i) $\tilde{\boldsymbol{v}}^{n+1/2}=\boldsymbol{v}^{n-1/2}+(\Delta t/2)[\overline{\boldsymbol{a}^{n-1}}+(\tilde{\boldsymbol{v}}^{n+1/2}+\boldsymbol{v}^{n-1/2})\times\boldsymbol{\Omega}^{n}]$;

(ii) $\tilde{\boldsymbol{x}}^{n+1}=\boldsymbol{x}^{n}+\tilde{\boldsymbol{v}}^{n+1/2}\Delta t$;

(iii) $\tilde{\boldsymbol{x}}^{n+1}\rightarrow\tilde{\rho}^{n+1}\boldsymbol{\chi}$ (interpolation of charge density and matrix coefficient from the particles), where $\boldsymbol{\chi}$ represents the effective polarizability related to $\tilde{\rho}^{n+1}$ and $\boldsymbol{\Omega}^{n}$.[24]

(iv) Solving the implicit Poisson equation to obtain $\boldsymbol{E}^{n+1}$ at the mesh, that is,

$$\nabla^{2}[(1+\boldsymbol{\chi})\cdot\phi^{n+1}]=-\tilde{\rho}^{n+1}/\varepsilon_{0}.\tag{6}$$

Final-pusher:

(v) $\boldsymbol{a}^{n+1}(\boldsymbol{x}^{n+1})\cong(q/m)\boldsymbol{E}^{n+1}(\tilde{x}^{n+1})$ (interpolation of the field from mesh);

(vi) $\delta\boldsymbol{v}=(\Delta t/2)[\boldsymbol{a}^{n+1}(\boldsymbol{x}^{n+1})+\delta\boldsymbol{v}\times\boldsymbol{\Omega}^{n}]$;

(vii) $\boldsymbol{v}^{n+1/2}=\tilde{v}^{n+1/2}+\delta\boldsymbol{v}$;

(viii) $\boldsymbol{x}^{n+1}=\tilde{x}^{n+1}+\delta\boldsymbol{v}\Delta t$;

(ix) $\overline{a^{n}}=\frac{1}{2}\overline{a^{n-1}}+\frac{1}{2}\boldsymbol{a}^{n+1}(\boldsymbol{x}^{n+1})$;

(x) $\boldsymbol{\Omega}^{n+1}=(q/m)\boldsymbol{B}^{n+1}(\boldsymbol{x}^{n+1})$ (interpolation of the field from mesh).

The dispersion relationship for the electrostatic Langmuir wave with an eigen-frequency of ω_{pe} described by DIMPIC is given by the following equation:[30]

$$(2z-1)(z-1)^{2}=-\omega_{\mathrm{pe}}^{2}\Delta t^{2}z^{3},\tag{7}$$

where $z\equiv\mathrm{e}^{-\mathrm{i}\omega\Delta t}$ and ω represents the frequency predicted by numerical simulations. By numerically solving Eq. (7), one can obtain the relationship between the amplitude $|z|$ and $\omega_{\mathrm{pe}}\Delta t$, which shows that the amplitude is damped and the numerical stability is independent of the time-step Δt. Besides, the damping of the wave is also helpful to suppress the grid heating caused by a large spatial step with poor resolution in Debye length.

It can be seen that DIMPICs allow the use of large spatial and temporal steps while maintaining numerical stability, which is not possible in EXPICs. However, the latter method has a simpler particle pusher. Additionally, DIMPIC has a more complex algorithm, and has a lower efficiency in solving the implicit Poisson equations as compared to solving the explicit Poisson equations. It becomes more challenging to solve such implicit equations in the high dimensional magnetized plasma systems because $\boldsymbol{\chi}$ is now anisotropic. In addition, the parallelism strategies for DIMPIC and EXPIC are different. For explicit PICs, significant CPU time gains can be obtained by only paralleling particle process since most of the CPU time is related to the particles.[9] For the direct implicit PICs, however, it is very important to parallel solve both the field solving process and particle process, because the time of field solving here takes a significant fraction of the total simulation time.[20] Meanwhile, parallel solving the implicit Poisson equation is troublesome due to the time-dependent matrix coefficients $\boldsymbol{\chi}$.

3. Descriptions of damped explicit PIC method

The descriptions of the new method are started with the central difference equations of motion used in DIMPIC, and one can still suppose

$$\boldsymbol{a}^{n}(\boldsymbol{x}^{n})=\frac{1}{2}\boldsymbol{a}^{n+1}(\boldsymbol{x}^{n+1})+\frac{1}{2}\overline{\boldsymbol{a}^{n-1}}.$$

As mentioned before, the traditional DIMPIC solves the implicit Poisson equation first to obtain an approximate field

$\boldsymbol{E}^{n+1}$. Then, the approximate $\boldsymbol{a}^{n+1}(\boldsymbol{x}^{n+1})$ is obtained by both this estimated $\boldsymbol{E}^{n+1}$ and the quantity $\tilde{x}^{n+1}$ provided by the pre-pusher, using some interpolation algorithms. Here, however, we adopt a different strategy. Firstly, we give an approximate $\tilde{a}^{n+1}(\boldsymbol{x}^{n+1})$, and then pre-push the particle to obtain the approximate field $\boldsymbol{E}^{n+1}$ by solving an explicit Poisson equation. Finally, we re-obtain an approximate $\boldsymbol{a}^{n+1}(\boldsymbol{x}^{n+1})$ to finish the push process.

To obtain $\boldsymbol{a}^{n+1}(\boldsymbol{x}^{n+1})$, we suppose that an estimated $\tilde{a}^{n+1}(\boldsymbol{x}^{n+1})$ is already known. It is reasonable to set the estimated $\tilde{a}^{n+1}(\boldsymbol{x}^{n+1})$ as follows:

$$\tilde{a}^{n+1}(\boldsymbol{x}^{n+1}) = 2\boldsymbol{a}^{n}(\boldsymbol{x}^{n}) - \overline{\boldsymbol{a}^{n-1}}. \tag{8}$$

Here the known quantity $\boldsymbol{a}^{n}(\boldsymbol{x}^{n})$ represents the electric field acceleration of the particle at previous calculation step. As a result, one can re-obtain an approximate $\tilde{a}^{n}(\boldsymbol{x}^{n})$ at current time step through the relationship $\tilde{a}^{n}(\boldsymbol{x}^{n}) = \frac{1}{2}\tilde{a}^{n+1}(\boldsymbol{x}^{n+1}) + \frac{1}{2}\overline{a^{n-1}}$. It can be seen that the $\tilde{a}^{n}(\boldsymbol{x}^{n})$ here is actually equal to the known $\boldsymbol{a}^{n}(\boldsymbol{x}^{n})$. The second step is to use the known $\tilde{a}^{n}(\boldsymbol{x}^{n})$ to explicitly push the particle and obtain a charge density $\tilde{\rho}^{n+1}$ based on the information about the particles in the future. Then, the field $\boldsymbol{E}^{n+1}$ is obtained by solving the explicit Poisson equation with the source term $\tilde{\rho}^{n+1}$. Now, one gets a new $\boldsymbol{a}^{n+1}(\boldsymbol{x}^{n+1})$ and a new $\boldsymbol{a}^{n}(\boldsymbol{x}^{n}) = \frac{1}{2}\boldsymbol{a}^{n+1}(\boldsymbol{x}^{n+1}) + \frac{1}{2}\overline{a^{n-1}}$. Finally, we push the particle again with the new $\boldsymbol{a}^{n}(\boldsymbol{x}^{n})$ and update the $\overline{a^{n-1}}$ as $\overline{a^{n}} = \frac{1}{2}\boldsymbol{a}^{n+1}(\boldsymbol{x}^{n+1}) + \frac{1}{2}\overline{a^{n-1}}$.

One can also set the estimated $\tilde{a}^{n+1}(\boldsymbol{x}^{n+1})$ as zero or $\boldsymbol{a}^{n}(\boldsymbol{x}^{n})$, and these options will be discussed in Section 5. Here, however, we will estimate $\tilde{a}^{n+1}(\boldsymbol{x}^{n+1})$ using Eq. (8). The algorithm of the new PIC method is as follows: starting with the known quantities $\boldsymbol{v}^{n-1/2}$, $\boldsymbol{x}^{n}$, $\overline{a^{n-1}}$, $\boldsymbol{a}^{n}(\boldsymbol{x}^{n})$, and $\boldsymbol{\Omega}^{n}$:

Pre-pusher:

(i) $\tilde{a}^{n+1}\left(\boldsymbol{x}^{n+1}\right) = 2\boldsymbol{a}^{n}\left(\boldsymbol{x}^{n}\right) - \overline{a^{n-1}}$;

(ii) $\tilde{a}^{n}(\boldsymbol{x}^{n}) = \frac{1}{2}\tilde{a}^{n+1}\left(\boldsymbol{x}^{n+1}\right) + \frac{1}{2}\overline{a^{n-1}}$;

(iii) $\tilde{\boldsymbol{v}}^{n+1/2} = \boldsymbol{v}^{n-1/2} + \tilde{a}^{n}(\boldsymbol{x}^{n})\Delta t + (\Delta t/2)[(\tilde{\boldsymbol{v}}^{n+1/2} + \boldsymbol{v}^{n-1/2}) \times \boldsymbol{\Omega}^{n}]$;

(iv) $\tilde{x}^{n+1} = \boldsymbol{x}^{n} + \tilde{\boldsymbol{v}}^{n+1/2}\Delta t$;

(v) $\tilde{x}^{n+1} \to \tilde{\rho}^{n+1}$ (interpolation of charge density from the particles);

(vi) solving the explicit Poisson equation to obtain $\boldsymbol{E}^{n+1}$ at the mesh, that is,

$$\nabla^2\phi^{n+1} = -\tilde{\rho}^{n+1}/\varepsilon_0. \tag{9}$$

Final-pusher:

(vii) $\boldsymbol{a}^{n+1}(\boldsymbol{x}^{n+1}) \cong (q/m)\boldsymbol{E}^{n+1}(\tilde{x}^{n+1})$ (interpolation of the field from mesh);

(viii) $\delta\boldsymbol{a} = \boldsymbol{a}^{n+1}\left(\boldsymbol{x}^{n+1}\right) - \tilde{a}^{n+1}\left(\boldsymbol{x}^{n+1}\right)$;

(ix) $\delta\boldsymbol{v} = (\Delta t/2)[\delta\boldsymbol{a} + \delta\boldsymbol{v} \times \boldsymbol{\Omega}^{n}]$;

(x) $\boldsymbol{v}^{n+1/2} = \tilde{\boldsymbol{v}}^{n+1/2} + \delta\boldsymbol{v}$;

(xi) $\boldsymbol{x}^{n+1} = \tilde{x}^{n+1} + \delta\boldsymbol{v}\Delta t$;

(xii) $\overline{a^{n}} = \frac{1}{2}\overline{a^{n-1}} + \frac{1}{2}\boldsymbol{a}^{n+1}(\boldsymbol{x}^{n+1})$;

(xiii) $\boldsymbol{\Omega}^{n+1} = (q/m)\boldsymbol{B}^{n+1}(\boldsymbol{x}^{n+1})$ (interpolation of the field from mesh).

It can be seen from the above loop that the unknown future electric field is now obtained by solving an explicit Poisson equation with source term obtained by the position from explicitly propulsion of the particle. In addition, the new method can damp high-frequency plasma oscillation strongly, as described below. For these reasons, the new PIC method is namely as damped explicit PIC (DEXPIC). For the new method, solving the Poisson equation parallel is expected to be easier due to the time-independent matrix coefficients. Figure 1 shows the differences between the flowchart of DEXPIC and that of the DIMPIC in the case where magnetic field is ignored.

In the following studies, we will examine the numerical accuracy and stability of the DEXPIC method. Furthermore, we will demonstrate that the method maintains the desirable damping of high-frequency electronic oscillation, while accurately describes low-frequency phenomena.

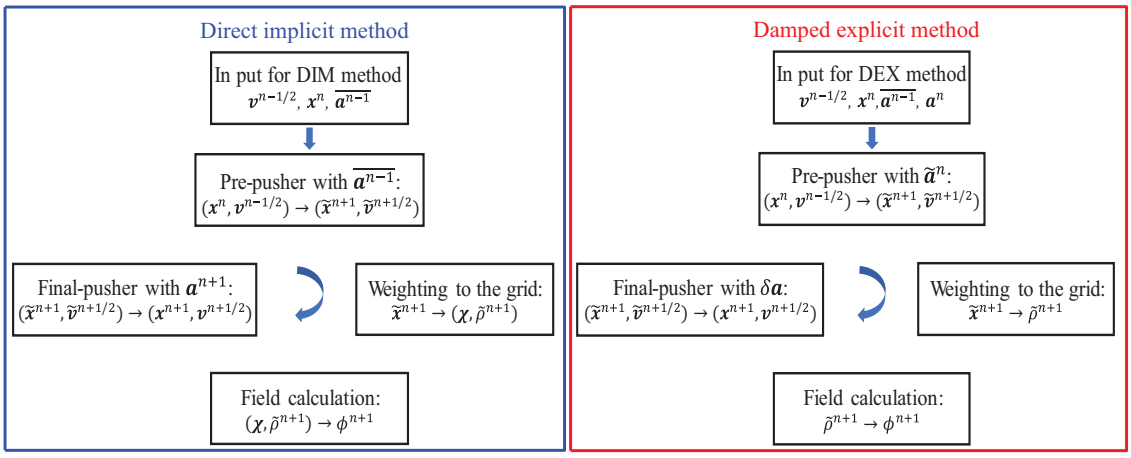


Fig. 1. Differences between the flowchart of the DEXPIC and that of the DIMPIC.

4. Numerical experiments

In this section, several numerical experiments will be performed to check the performance of the DEXPIC, including the motion of charged particles in EM fields, magnetized plasma sheath, and free diffusion of magnetized plasma into vacuum.

4.1. Particle pusher test

The motion of a charged particle in EM fields is first tested to check the accuracy of the particle pusher. We consider a test particle with mass $m = 1$ and charge $q = -1$ that moves in an electric field varying with x and a constant static magnetic field:

$$\boldsymbol{E} = (1+0.1x, 0, 0), \quad \boldsymbol{B} = (0, 0, 1). \tag{10}$$

At the beginning, the particle enters the computational domain with position $(0,0,0)$ and velocity $(0,0,0)$. The test runs until the total simulation time $T = 12$.

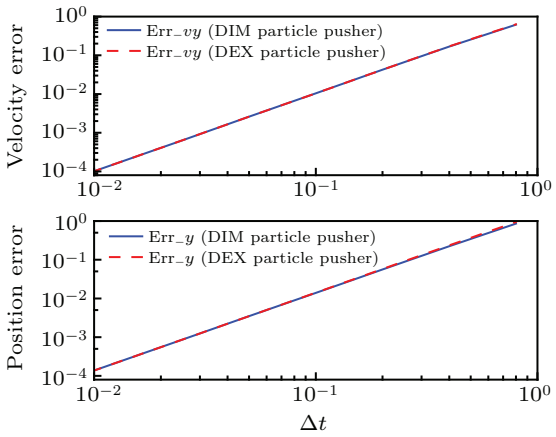


Fig. 2. Accuracy analysis of the DEX particle pusher. The errors increase with the time-step, and show second-order accuracy.

To analyze the accuracy of the particle pusher with varying time-steps, we use three methods to calculate the trajectory of the particle. The first method, denoted as #1, solves the equations of motion through ODE solvers with a small time-step of $\Delta t = 1.25 \times 10^{-4}$, which provides the equivalent analytical solutions. The other two methods are the DIM particle pusher and the DEX particle pusher, where different time-steps are used. The following relationship is introduced to analyze the accuracy of the particle pusher with respect to the time-step:[31]

$$\begin{aligned} \mathrm{Err_}x &= \sqrt{\sum\nolimits_n \left|\boldsymbol{x}^n_{\mathrm{test}} - \boldsymbol{x}^n_{\mathrm{ref}}\right|^2 \Delta t}, \\ \mathrm{Err_}v &= \sqrt{\sum\nolimits_n \left|\boldsymbol{v}^n_{\mathrm{test}} - \boldsymbol{v}^n_{\mathrm{ref}}\right|^2 \Delta t}. \end{aligned} \tag{11}$$

Here $\boldsymbol{x}^n$ and $\boldsymbol{v}^n$ represent the position and velocity at time-step n. The subscript 'test' indicates that the data are obtained by the DIM particle pusher or DEX particle pusher, while 'ref' represents the reference value provided by the method #1. The logarithmic plots of the errors $E_{\mathrm{rr_}y}$ and $E_{\mathrm{rr_}vy}$ as a function of time-step are shown in Fig. 2. It can be seen that the errors of both the DIM particle pusher and the DEX particle pusher increase with the time step, and show the second-order accuracy.

In addition, it is necessary to check the numerical stability of the DEX particle pusher. To do so, we consider the analysis of the electrostatic Langmuir wave.[3] In this case, the central difference equations of the motion are given by

$$\begin{aligned} &\frac{\boldsymbol{v}^{n+1/2} - \boldsymbol{v}^{n-1/2}}{\Delta t} \\ &= \frac{1}{2}\left[\boldsymbol{a}^{n+1}\left(\boldsymbol{x}^{n+1}\right) + \frac{\boldsymbol{v}^{n-1/2} - \boldsymbol{v}^{n-3/2}}{\Delta t}\right], \\ &\frac{\boldsymbol{x}^{n+1} - \boldsymbol{x}^n}{\Delta t} = \boldsymbol{v}^{n+1/2}, \end{aligned} \tag{12}$$

for simple harmonic oscillation with frequency of ω_{pe}, one can derive the following expression:[32]

$$\boldsymbol{a}^{n+1}(\boldsymbol{x}^{n+1}) = -\omega^2_{\mathrm{pe}}\boldsymbol{x}^{n+1} \cong -\omega^2_{\mathrm{pe}}\tilde{x}^{n+1}, \tag{13}$$

where $\tilde{x}^{n+1} = \boldsymbol{x}^n + \boldsymbol{v}^{n-1/2}\Delta t + \tilde{a}^n(\boldsymbol{x}^n)\Delta t^2$ represents the position offered by the pre-pusher of the DEXPIC, and $\tilde{a}^n(\boldsymbol{x}^n) = \boldsymbol{a}^n(\tilde{x}^n) \cong -\omega^2_{\mathrm{pe}}\boldsymbol{x}^n$. Now, let us assume that the evolution of position over time is harmonic so that $\boldsymbol{x}^n = \boldsymbol{x}_0 z^n$, where $\boldsymbol{x}_0$ represents the initial position and $z^n \equiv \mathrm{e}^{-\mathrm{i}\omega n\Delta t}$.[33] Here, ω is the mode frequency obtained by simulation.

Bring Eq. (13), $\tilde{x}^{n+1} = \boldsymbol{x}^n + \boldsymbol{v}^{n-1/2}\Delta t + \tilde{a}^n(\boldsymbol{x}^n)\Delta t^2$, $\tilde{a}^n(\boldsymbol{x}^n) \cong -\omega^2_{\mathrm{pe}}\boldsymbol{x}^n$, and $\boldsymbol{x}^n = \boldsymbol{x}_0 z^n$ into Eq. (12), and finally we obtain the approximate dispersion relationship for the electrostatic Langmuir wave as

$$(2z-1)(z-1)^2 = -\omega^2_{\mathrm{pe}}\Delta t^2[(2-\omega^2_{\mathrm{pe}}\Delta t^2)z^2 - z]. \tag{14}$$

Equation (14) shows that the DEXPIC is numerical unstable when $\omega_{\mathrm{pe}}\Delta t > 1$ because one has $|z| > 1$ now. It is worth noting that the dispersion relationship described by Eq. (14) is approximate because the value of $\boldsymbol{a}^{n+1}(\boldsymbol{x}^{n+1})$ is estimated at $\tilde{x}^{n+1}$ rather than $\boldsymbol{x}^{n+1}$. In the actual tests, we have found that the stability constraint on time-step is more restrictive, as shown in the Subsection 4.2.

4.2. Magnetized plasma sheath

We have implemented the DEX particle pusher in a custom short electrostatic PIC code with one-dimensional (1D) in space and three-dimensional (3D) in velocity. In this subsection, we will use the DEXPIC to simulate magnetized plasma sheath for the following purposes. Firstly, the numerical stability constraint on time-step of the DEXPIC will be derived from the experimental data. Secondly, we will observe how well the DEXPIC does at damping high-frequency electron oscillations, and what consequences such damping might have. To analyze the performance of the new method, we will compare the results obtained by DEXPIC with those obtained by the standard EXPIC and the DIMPIC.

In all tests, we assume the ions are immobile, and only consider the dynamics of electrons. At the beginning, a 1D uniform plasma plate with electron number density of 1×10^{16} m^{-3} and Maxwell velocity distribution for electrons with temperature of 1 eV is distributed between two parallel electrodes placed along the x direction. Meanwhile, a constant transverse static magnetic field B_z is present, and the potential of the electrodes is set zero. Additionally, every particle that reaches the electrodes will be absorbed and removed from the simulation. Moreover, no secondary electron emission, electron reflection, and particle–particle collisions are considered. The simulation time is normalized to $1/\omega_{\rm pe}$.

In first test #1, we use the following parameters to find the required constraint for numerical stability: system length $L=120\lambda_{\rm De}$, 30 uniformly spaced grid points, 256 macro-particles per grid, $B_z=10$ Gs (1 Gs$=10^{-4}$ T), and tunable time-steps. The simulations run for time of 10000. Figure 3 shows the time history of the center potential predicted by the DEXPIC. One can observe obviously numerical instability when $\omega_{\rm pe}\Delta t=0.895$. In fact, when $\omega_{\rm pe}\Delta t\le0.894$, we do not observe numerical instability in simulations run for long time (up to millions plasma oscillation period). It is worth noting that the CFL condition is ensured in all tests.

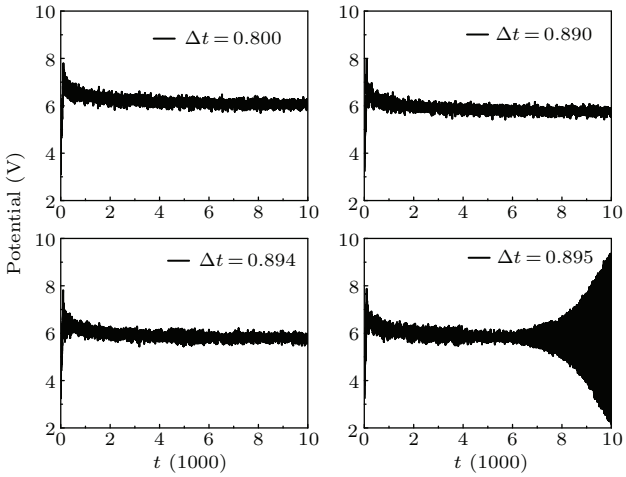


Fig. 3. Time history of the center potential predicted by the DEXPIC with different time-steps. One can observe the numerical instability when $\omega_{\rm pe}\Delta t=0.895$.

As shown in Fig. 3, the desired numerical stability at large time-step cannot be ensured by the DEXPIC. However, this method can still damp high-frequency oscillation significantly and suppresses the numerical instability originating from the coarse spatial resolution in the Debye length. As a result, the DEXPIC is stable when a large spatial step is used, as shown in the following studies.

Now we consider the second test #2 using the following parameters: system length $L=30\lambda_{\rm De}$, 30 uniformly spaced grid points, 256 macro-particles per cell, time-step $\omega_{\rm pe}\Delta t=0.2$, and $B_z=10$ Gs. The simulations run for time of 1000. Figure 4 shows the time history of the center potential obtained by three methods, in which the illustration shows the history from $t=900$ to $t=1000$. For the EXPIC, the time history shows a stable numerical oscillation, which actually captures the electron plasma oscillation.[34] If a large spatial step ($\Delta x\gg\lambda_{\rm De}$) is used, then such numerical oscillation will be amplified and result in significant fine-grid-instability.[3] However, the EXPIC cannot damp such high-frequency oscillation very well, as shown in the blue line. As a result, it must use a very small spatial step, even when the electron plasma oscillation is no longer important.

On the other hand, the DIMPIC is a well-known method with damping of high-frequency wave.[28] Therefore, the time history obtained by the DIMPIC shows that the numerical oscillation weakens gradually over time, as shown by the red line. Interestingly, for the DEXPIC, the time history shows a similar result to that of the DIMPIC, proving that this method can also damp the high-frequency plasma oscillation, thereby suppress possible numerical instability. Now, it has been demonstrated that DEXPIC is a damped PIC method by comparing the time history of the center potential obtained by the three methods.

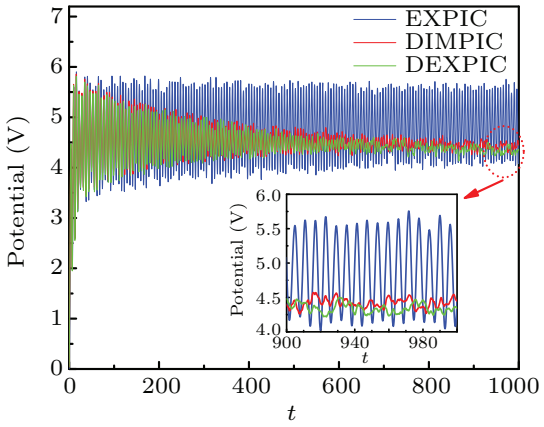


Fig. 4. The time history of the center potential obtained by three methods. The electron plasma oscillation is damped by both DIMPIC and DEXPIC.

The damping property of the DEXPIC also apply to the energy of the particles, as shown in Fig. 5, which shows the time history of electron number, electron kinetic energy $E_{\rm K}=\frac{1}{2}\sum_{i=1}^{N_{\rm e}}w_{\rm e}m_{\rm e}v_i^2$ and electric field energy $E_{\rm P}=\frac{1}{2}\varepsilon_0\sum_{j=1}^{N_{\rm g}}E_j^2{\rm d}V$. Here, $w_{\rm e}$ represents the weight of the macro-electrons, $N_{\rm e}$ is the electron number, v_i is the velocity of electron i, $N_{\rm g}$ is grid number, E_j is electric field at grid j and ${\rm d}V$ is the volume of each cell. All energies have been normalized to 10^{-7}. It can be seen that the EXPIC is not convergent because the electron number reduces over time gradually, indicating numerical heating of the electrons in long simulations. However, the energy of the system obtained by the EXPIC is conserved well. On the other hand, both the DIMPIC and DEXPIC are convergent, but at the cost of a gradual decrease in the energy of the particles over time.

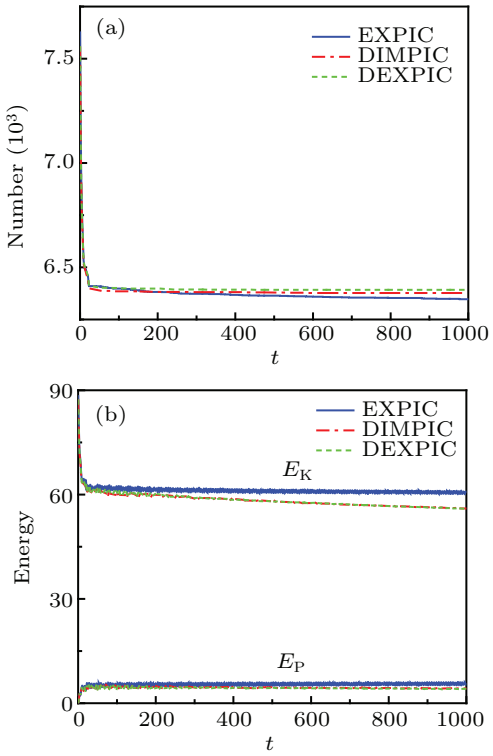


Fig. 5. Damping of the DEXPIC on the energy of the particles. (a) The time history of electron number. (b) The time history of electron kinetic energy and electric field energy.

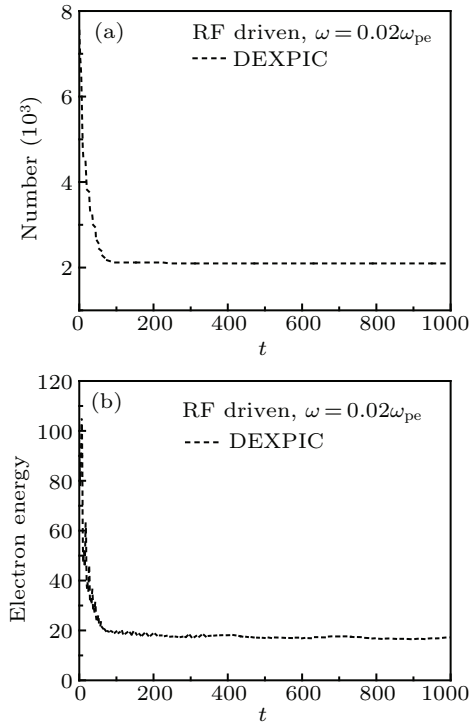


Fig. 6. (a) The time history of electron number. (b) The time history of electron kinetic energy. One electrode is driven by a voltage source with amplitude of $200(T_e/e)$ and frequency of $0.02\omega_{pe}/(2\pi)$. In this case, the plasma is dominated by low-frequency force fields and the cooling is tolerable.

The reduction of the energy is related to the numerical cooling. The cooling rate depends on $\omega_{tr}\Delta t$, where ω_{tr} represents the frequency of motion of the particles following the force fields.[30] As a result, the energy decreases while the particle number remains constant. The errors caused by such numerical cooling may lead to incorrect results. However, the cooling mentioned above is tolerable when $\omega_{tr}\Delta t$ is small. In other words, such numerical cooling is expected to be ignored when plasma is dominated by low-frequency force fields, such as radio frequency (RF) fields. For example, if we apply a voltage source with amplitude of $V = V_0\sin(\omega t)$ to one electrode, where $V_0 = 200(T_e/e)$ and $\omega = 0.02\omega_{pe}$, then the cooling is tolerable, as shown in Fig. 6.

The damping of high-frequency plasma oscillation favor suppression of finite-grid-instability resulting from the coarse spatial resolution in the electron Debye length. To prove this conclusion, we consider the third test #3: system length $L = 150\lambda_{De}$, 30 uniformly spaced grid points ($\Delta x = 5\lambda_{De}$), 256 macro-particles per cell, time-step $\omega_{pe}\Delta t = 0.8$, and $B_z =$ 30 Gs. The simulations run for time of 1000. The time history of the center potential and the total energy of the system obtained by three methods are plotted in Fig. 7.

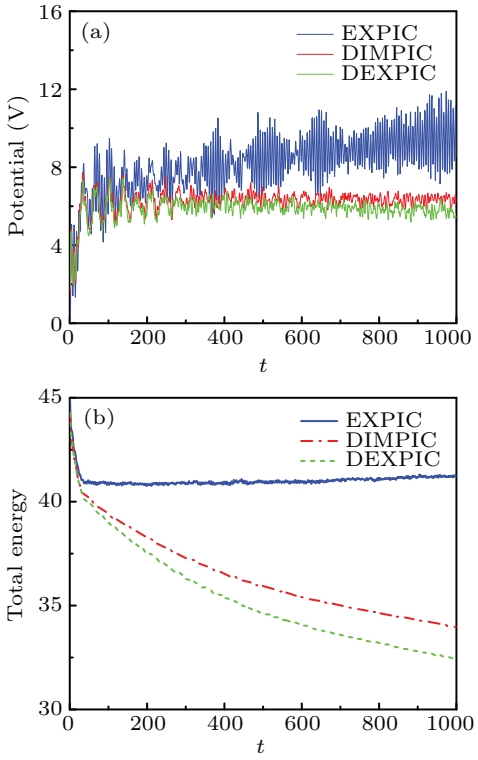


Fig. 7. (a) The time history of the center potential. (b) The time history of total energy of the system. The EXPIC now is unstable due to the fine-grid-instability resulting from the coarse spatial resolution in the electron Debye length.

In this test, the spatial step is large enough so it causes significant fine-grid-instability, which results in the instability of EXPIC. Both the amplitude of the potential and the total energy of the system obtained by the EXPIC increase with time, as indicated by the blue line in Fig. 7. In contrast, both DIMPIC and DEXPIC remain stable as they damp the numerical oscillation, as shown in the red and green lines in Fig. 7(a). Meanwhile, it seems that the damping provided by DEXPIC

is stronger than that provided by DIMPIC, as shown in the red dot-dashed line and the green dashed line in Fig. 7. In addition, the damping of both DIMPIC and DEXPIC in this case is stronger due to the larger time-step. Of course, when the plasma is dominated by low-frequency fields, the numerical cooling will be tolerable, as mentioned in test #2.

4.3. Free diffusion of magnetized plasma into vacuum

In Subsection 4.2, we have evaluated the performance of the DEXPIC using the magnetized plasma sheath, in which the plasma is dominated by the high-frequency electron plasma oscillation. The results show that the DEXPIC can damp the numerical oscillation strongly and suppress fine-grid-instability. Here, we consider another experiment in which the physical process depends on low-frequency bipolar electric fields, specifically free diffusion of plasma into vacuum.[35] In all tests, we consider a 1D uniform plasma plate with thickness of D placed at the center of the computational domain, with number density of 1×10^{16} m^{-3}, Maxwell velocity distribution for both electrons and ions, $T_e = T_i = 1$ eV and $m_i/m_e = 900$. The constant transverse static magnetic field is equal to 30 Gs. The particle boundary and potential boundary are the same as that in Subsection 4.2.

In the first test #1, the simulations run with the following parameters: system length $L = 1000\lambda_{De}$ and $D = 100\lambda_{De}$. The EXPIC uses 2000 uniformly spaced grid points, $\omega_{pe}\Delta t = 0.1$ and 256 macro-particles per cell, and its simulation results are treated as standard data. Both the DIMPIC and DEXPIC use 200 uniformly spaced grid points, $\omega_{pe}\Delta t = 0.8$ and 2560 macro-particles per cell. All simulations run until $t = 1000$, and the system length is long enough so that the total particle number remain constant in the simulations.

Figure 8 shows the evolution of the bipolar electric field over time obtained by three methods, where the field has been normalized to T_e/λ_{De}. It can be seen that the results offered by three methods agree well. Initially, the electrons in the outer layer of the plasma escape from the bulk region at fast speeds, leaving a shell full of positive charge density, which is surrounded by negative charge density.[23] As a result, one can observe an ambipolar electric field near this shell. On the other hand, the shell will be filled with negative charge density and be surrounded by positive charge density when the simulations run for longer term, because the drift velocity of the electron group is slower than that of ion group due to the effect of the transverse magnetic field.[1] Therefore, the direction of the bipolar field has reversed. It should be noted that the results obtained by both the DIMPIC and DEXPIC provide a correct description of the evolution of the bipolar fields over time, even they have poor spatial resolution.

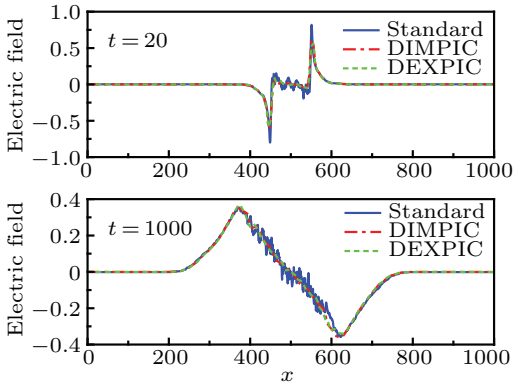


Fig. 8. The evolution of the bipolar electric field over time, in which the results obtained by three methods agree well.

The velocity distributions of electrons and ions at $t = 1000$ are plotted in Fig. 9, along with the initial distributions at $t = 0$ represented by the black line, where the velocity has been normalized to the initial average velocity $\bar{v}$, and the velocity space is [0, 4], discretized by 100 cells. The ambipolar fields tend to pull back the escaped charged particles towards the bulk region, while accelerate the charged particles in the outer layer of the plasma.[1] As a result, the velocity distributions of both electrons and ions are modulated. The figure demonstrates that the average velocity of electrons increases, while that of ions decreases, with the results obtained by three methods showing good agreement.

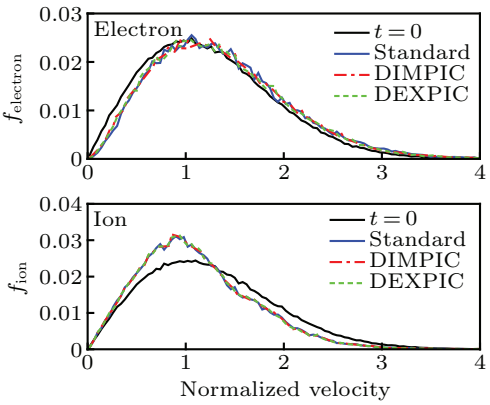


Fig. 9. The velocity distributions of electron and ion at $t = 1000$. The average velocity of electrons increases while that of ions decreases due to the effect of ambipolar field. The results obtained by the three methods agree well.

Figure 10 shows the time history of the total energy of the system obtained by three methods, in which the green dot-line represents the results obtained by the EXPIC using the same parameters as that used in DIMPIC and DEXPIC. It can be seen that the standard result shows good energy conservation. On the other hand, the result obtained by the EXPIC using poor resolution in Debye length and high frequency electron plasma oscillation shows that the total energy raises over time, which indicates numerical instability in the simulations run for long time. As a comparison, the total energy obtained by both DIMPIC and DEXPIC decreases rapidly firstly and stabilizes

gradually over time. The decreased energy originates from the numerical cooling mentioned before. As time increases, the plasma gradually becomes dominated by low-frequency bipolar electric field so that the cooling is tolerate. Again, the figure indicates that the DEXPIC provides stronger damping compared to that of DIMPIC. The stronger damping may be beneficial when larger space step or fewer macro-particles per cell is used, as it can suppress the heating caused by numerical noise more effectively.

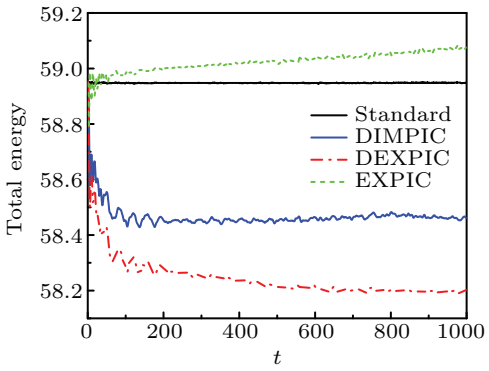


Fig. 10. The time history of the total energy of the system obtained by three methods. The total energy predicted by the EXPIC increases over time.

Now, we consider the second test #2 to check the accuracy of the DEXPIC using the spatial step and time-step with different resolutions in Debye length and high-frequency electron plasma oscillation. The simulations run with the following parameters: system length $L = 1000\lambda_{\mathrm{De}}$, $D = 100\lambda_{\mathrm{De}}$, and the total simulation time is equal to 1000. The EXPIC uses the same spatial step and time-step as that in test #2. Both the DIMPIC and DEXPIC use 200, 250, 320, 400, 500, 625, and 1000 uniformly spaced grid points respectively, and the total particle number is the same as that of the EXPIC so that the initial velocity distribution function is constant. The time-steps used in the DIMPIC and DEXPIC are varied with spatial step to ensure $v_{\mathrm{the}}\Delta t/\Delta x$ is constant so that CFL condition is constant, where v_{the} represents the thermal velocity of electrons. However, when $\Delta x = 5\lambda_{\mathrm{De}}$, the time-step is set as $\omega_{\mathrm{pe}}\Delta t = 0.8$ rather than $\omega_{\mathrm{pe}}\Delta t = 1.0$ since the stability constraint on the time-step of the DEXPIC requires $\omega_{\mathrm{pe}}\Delta t \leq 0.894$.

To calculate the accuracy, we determine the error $\varepsilon(f_{\mathrm{e}})$ in the velocity distribution function f_{e} of the electrons using the following relation:

$$\varepsilon(f_{\mathrm{e}}) = \sqrt{\int |f_{\mathrm{test}} - f_{\mathrm{ref}}|^2 \Delta v}, \tag{15}$$

where f_{ref} represents the reference distribution function taken from the standard EXPIC. The integral element Δv is 0.04. Equation (15) is actually another version of Eq. (11). The differences between the distribution function obtained by three methods are shown in Fig. 11. It can be seen from the figure that the accuracy of both DIMPIC and DEXPIC is acceptable as the resolution in Debye length and high frequency electron plasma oscillation gets worse, in which the maximum error of the DEXPIC is only around 0.15%. It should be noted here that both the DIMPIC and DEXPIC use the same total particle number as that used by the standard EXPIC, which means that the number of the macro-particles per cell increases as the number of grids decreases. The increased number of the macro-particles per cell helps reduce numerical errors.[10]

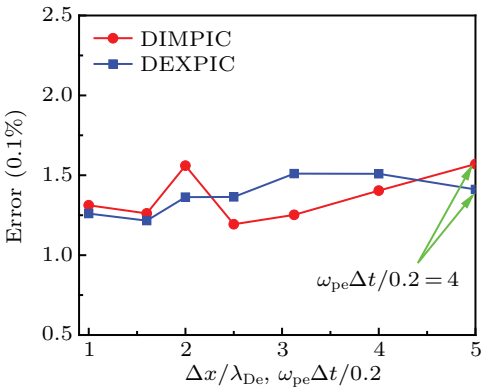


Fig. 11. Differences between the results obtained by standard EXPIC, DIMPIC, and DEXPIC. The accuracy of the DIMPIC and DEXPIC is acceptable when the resolution in Debye length and high frequency electron plasma oscillation gets worse.

Table 1. The evolution of the computation time spent by DIMPIC and DEXPIC, as a function of spatial step and time-step. The CPU time spent by the standard EXPIC is equal to 53.632 s.

Case	Δx	Δt	cycle	DIMPIC (s)	DEXPIC (s)
1	1.000	0.200	1000	43.150	32.803
2	1.600	0.320	1000	27.331	20.181
3	2.000	0.400	1000	21.333	16.150
4	2.500	0.500	1000	17.191	12.862
5	3.125	0.625	1000	13.730	10.344
6	4.000	0.800	1000	10.761	8.233
7	5.000	0.800	1000	10.670	7.773

Both figures 9 and 11 show that the DEXPIC can describe the modulation of the bipolar electric fields to the velocity distribution function of charged particles accurately, as the DIMPIC does. More importantly, the DEXPIC takes less computation time compared to that of the DIMPIC, as shown in Table 1, which shows the evolution of the computation time spent by the two methods as a function of spatial step and time-step. Here, the CPU time spent by the standard EXPIC is equal to 53.632 s. For both DIMPIC and DEXPIC, when they push the particles, we do not calculate the magnetic field felt by the particles based on their positions, because the magnetic field here is uniform. For the DIMPIC, however, we calculate the magnetic field felt by each particle according to their positions before solve the implicit Poisson equation and consider the contribution of the charge and magnetic field carried

by each particle to the total polarizability χ, to simulate the plasma with non-uniform magnetic fields, even the magnetic field here is actually uniform. It can be seen that the DEXPIC runs faster than DIMPIC in all cases. Compared with DEXPIC, the additional computational time required by DIMPIC is almost used to calculate the polarizability of electrons and ions.

5. More discussions and the future of work

In conclusion, we proposed a damped explicit PIC method in this work to improve the computational speed of traditional direct implicit methods in the research of bounded plasma. The new method obtains the future electric field by solving explicit Poisson equation with source term obtained by the position from explicitly propulsion of the particles, and provides stronger damping of high-frequency numerical oscillation compared to that provided by the direct implicit method. However, the new method cannot ensure numerical stability when very large time-steps are used. Nonetheless, it can still suppress numerical instability originating from the poor resolution in Debye length and high frequency electron plasma oscillation significantly. In tests, the performance of the damped method using a large spatial step $\Delta x = 5\lambda_{\mathrm{De}}$ and a large time-step $\omega_{\mathrm{pe}}\Delta t = 0.8$ is well while that of the traditional explicit method using the same parameters is poor.

The damped explicit method may be useful in certain specific plasma studies, such as magnetron discharges, where a small time-step $\omega_{\mathrm{ce}}\Delta t = 0.2$ is required to capture the dynamics of the system accurately,[36] where ω_{ce} represents electron cyclotron frequency. In this case, the advantages of traditional direct implicit methods are limited since a very large time-step $\omega_{\mathrm{ce}}\Delta t \gg 0.2$ is not allowed. Therefore, the new damped method is expected to be a better choice because its field solver is more efficient, and it provides stronger damping of numerical heating when larger spatial steps are used.

Other estimated future acceleration $\tilde{a}^{n+1}(\boldsymbol{x}^{n+1})$ can be used in the damped method. For example, one can set the estimated $\tilde{a}^{n+1}(\boldsymbol{x}^{n+1})$ as zero or $\boldsymbol{a}^n(\boldsymbol{x}^n)$, as mentioned in Section 3, and the differences between the results obtained by the damped method using different estimated $\tilde{a}^{n+1}(\boldsymbol{x}^{n+1})$ can be observed in terms of damping, as shown in Fig. 12, which displays the time history of the total energy of the system described in the test #3 in the numerical experiment of plasma sheath. It can be seen that the damping provided by the damped method using $\tilde{a}^{n+1}(\boldsymbol{x}^{n+1}) = 0$ is similar to that provided by the direct implicit method, while the damped method using $\tilde{a}^{n+1}(\boldsymbol{x}^{n+1}) = \boldsymbol{a}^n(\boldsymbol{x}^n)$ provides the strongest damping. In addition, if a smaller estimated $\tilde{a}^{n+1}(\boldsymbol{x}^{n+1})$ is used, then a larger time-step can be used because now the constraint is relaxed to $\omega_{\mathrm{pe}}\Delta t \leq 1.549$.

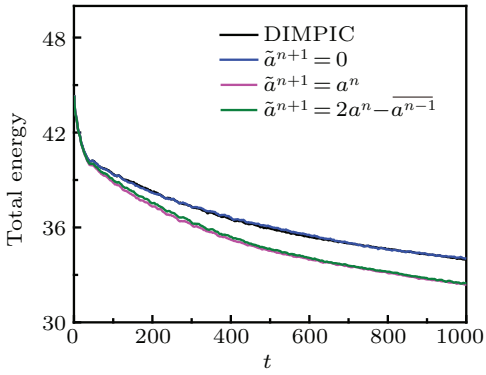


Fig. 12. The time history of the total energy of the system, where the simulation parameters are the same as those of the test #3 in the experiment of plasma sheath. The damped method using different estimated future accelerations produces different levels of damping.

Finally, the damped explicit PIC method is expected be coupled with Monte Carlo collision (MCC) method to form a damped explicit PIC/MCC method for simulate plasma discharge. In addition, the damped method with tunable damping is also attractive. The construction of rotational symmetry electrostatic damped explicit PIC/MCC method with tunable damping is a topic for future studies.

Acknowledgements

Project supported by the National Key Research and Development Program of China (Grant No. 2022YFE03050001), also partly by the National Natural Science Foundation of China (Grant No. 12175160), and the Project Funded by the Priority Academic Program Development of Jiangsu Higher Education Institutions (PAPD).

References

[1] Lieberman M A and Lichtenberg A J 2005 *Principles of Plasma Discharges and Materials Processing*, 2nd edn. (New York: Wiley)
[2] Liu Y X, Zhang Q Z, Zhao K, Zhang Y R, Gao F, Song Y H and Wang Y N 2022 *Chin. Phys. B.* **31** 085202
[3] Birdsall C K and Langdon A B 2005 *Plasma physics via computer simulation* (Taylor and Francis)
[4] Birdsall C K 1991 *IEEE Trans. Plasma Sci.* **19** 65
[5] Gudmundsson J T 2020 *Plasma Sources Sci. Technol.* **29** 113001
[6] Guo C Z, Wu H, Peng Y L, Wang Z J, Jiang W and Zhang Y 2022 *J. Phys. D: Appl. Phys.* **55** 465202
[7] Wang Y G, Ma X Q, Bouwman D, Liu Z R, Ebert U and Zhang X N 2022 *Plasma Sources Sci. Technol.* **31** 105015
[8] Zuo C Y, Gao F, Dai Z L and Wang Y N 2018 *Acta Phys. Sin.* **67** 225201 (in Chinese)
[9] Kawamura E, Birdsall C K and Vahedi V 2000 *Plasma Sources Sci. Technol.* **9** 413
[10] Deluzet F, Fubiani G, Garrigues L, Guillet C and Narski J 2022 *ESAIM: M2AN* **56** 1809
[11] Juhasz Z, Durian J, Derzsi A, Matejcik S, Donko Z and Hartmann P 2021 *Comput. Phys. Commun.* **263** 107913
[12] Yu K M, Kumar P, Yuan S H, Cheng A Q and Samulyak R 2022 *Comput. Phys. Commun.* **277** 108396

[13] Wang H Y, Jiang W and Wang Y N 2009 *Comput. Phys. Commun.* **180** 1305

[14] Adam J C, Gourdin-Serveniere A and Langdon A B 1982 *J. Comput. Phys.* **47** 229

[15] Taccogna F and Minelli P 2018 *Phys. Plasmas* **25** 061208

[16] Tonneau R, Pflug A and Lucas S 2020 *Plasma Sources Sci. Technol.* **29** 115007

[17] Szabo J, Warner N, Martinez-Sanchez M and Batishchev O 2014 *J. Propul. Power.* **30** 197

[18] Revel A, Minea T and Costin C 2018 *Plasma Sources Sci. Technol.* **27** 105009

[19] Welch D R, Rose D V, Clark R E, Genoni T C and Hughes T P 2004 *Comput. Phys. Commun.* **164** 183

[20] Markidis S, Lapenta G and Rizwan-uddin 2010 *Math. Comput. Simulat.* **80** 1509

[21] Vahedi V, DiPeso G, Birdsall C K, Lieberman M A and Rognlien T D 1993 *Plasma Sources Sci. Technol.* **2** 261

[22] Eremin D 2022 *J. Comput. Phys.* **452** 110934

[23] Gonzalez-Herrero D, Micera A, Boella E, Park J and Lapenta G 2019 *Comput. Phys. Commun.* **236** 153

[24] Lapenta G 2017 *J. Comput. Phys.* **334** 349

[25] Lei L, Jin X L, Li J B, Li L X and Li B 2022 *Phys. Plasmas* **29** 073904

[26] Garrigues L, Du Montcel B T, Fubiani G, Bertomeu F, Deluzet F and Narski J 2021 *J. Appl. Phys.* **129** 153303

[27] Tskhakaya D, Matyash K, Schneider R and Taccogna F 2007 *Contrib. Plasma Phys.* **47** 563

[28] Friedman A 1990 *J. Comput. Phys.* **90** 292

[29] Langdon A B, Cohen B I and Friedman A 1983 *J. Comput. Phys.* **51** 107

[30] Cohen B I, Langdon A B and Friedman A 1982 *J. Comput. Phys.* **46** 15

[31] Bai J W, Cao Y, Chu Y C and Zhang X 2018 *Comput. Math. Appl.* **75** 1887

[32] Dendy R O 1990 *Plasma dynamics* (Oxford University Press)

[33] Isaacson E and Keller H B 1994 *Analysis of numerical methods* (Courier Corporation)

[34] Liu H T, Quan L L, Chen Q, Zhou S J and Cao Y 2020 *Phys. Rev. E* **101** 043307

[35] Friedman A, Parker S E, Ray S L and Birdsall C K 1991 *J. Comput. Phys.* **96** 54

[36] Ryabinkin A N, Serov A O, Pal A F, Mankelevich Y A, Rakhimov A T and Rakhimova T V 2021 *Plasma Sources Sci. Technol.* **30** 055009